Electronic Supplementary Material (ESI) for Journal of Materials Chemistry A.

Supporting information

Transforming NiFe layered double hydroxide into $NiFeP_x$ for efficient alkaline water splitting

Jia Zhao[1], Nan Liao[1], Jingshan Luo*[1,2]

[1]*Institute of Photoelectronic Thin Film Devices and Technology, Solar Energy Research Center, Key Laboratory of Photoelectronic Thin Film Devices and Technology of Tianjin, Ministry of Education Engineering Research Center of Thin Film Photoelectronic Technology, Renewable Energy Conversion and Storage Center, Nankai University, 300350 Tianjin, China,*

[2]*Haihe Laboratory of Sustainable Chemical Transformations, 300192 Tianjin, China.*

Email: jingshan.luo@nankai.edu.cn

Experimental section

Preparation of NiFe LDH/Ni foam electrodes. The NiFe LDH/Ni foam electrodes were fabricated using a hydrothermal growth method according to our previous report with a slightly modified procedure. Briefly, 0.15 g $Ni(NO_3)_2$, 0.20 g $Fe(NO_3)_3$ and 0.3 g urea were mixed in 36 mL deionized water. After the reagents were dissolved, the solution was poured into a 50 mL autoclave with a piece of Ni foam placed against the wall. The growth was carried out at 120 °C in an electric oven for 6 h. After allowing the autoclave to cool naturally to room temperature, the samples were removed, washed with deionized water and dried naturally in ambient conditions.

Conversion of NiFe LDH into $NiFeP_x$. The NiFe LDH/Ni foam electrodes were transformed into $NiFeP_x$ through phosphidation in a tube furnace and NaH_2PO_2 was used as the phosphorous source. In detail, NiFe LDH/Ni foam electrodes and NaH_2PO_2 powder were placed at two separate positions in a tube furnace with NaH_2PO_2 located upstream. Typically, 1.0 g NaH_2PO_2 was used. Subsequently, the sample was heated at 350 °C for 2 h in a static N_2 atmosphere and then allowed to cool naturally to ambient temperature under N_2.

Material characterizations. A Rigaku (Japan) diffractometer (40 kV, 40 mA, 1600 W, with a Cu-target tube and a graphite monochromator) was used for powder X-ray diffractometry (PXRD) at room temperature. Scanning electron microscopy (SEM) images were obtained using a JSM-7800F field-emission scanning electron microscope (Jeol, Japan). Transmission electron microscopy (TEM), energy dispersive X-ray spectroscopy (EDS), and high-resolution TEM (HRTEM) were performed using a JEM-2800 microscope (Jeol, Japan). A Thermo Scientific ESCALAB 250Xi (Thermo, USA) X-ray photoelectron spectrometer with Al Kα (hv = 1486.6 eV) radiation was used to examine the oxidation states of the transition metals, with the adventitious carbon peak used to calibrate binding energies. The Inductively coupled plasma-optical emission spectroscopy (ICP-OES, Agilent 5110, USA) of samples was measured to evaluate the metal content in the catalysts.

In-situ **surface-enhanced Raman spectra (SERS).** The in-situ Surface Enhanced Raman spectra were acquired under controlled potentials using a three-electrode cell, which consisted of a working electrode at the top, a Pt plate counter electrode, and an Ag/AgCl reference electrode. The $NiFeP_x$ was prepared on the Ni foam which was sputtered with a 5 nm gold layer. All the Raman spectra were collected using Edinburgh Instruments. For all experiments, a laser with a 532 nm excitation wavelength and 10 mW power was used. Before the experiments were started, the Raman spectral shifts were calibrated routinely against the value of a silicon wafer (525 cm^{-1}). The exposure time was 2 s and the accumulation time was 200 s for one sample for a scan from -75 to 1575 cm^{-1}. The $NiFeP_x$ working electrodes were anodically scanned from OCP to 1.7 V *vs*. RHE.

Electrochemical characterizations. Using a three-electrode system, all electrochemical experiments were carried out using a CHI760E electrochemical workstation. The electrochemical performances of the catalyst electrodes towards oxygen evolution and hydrogen evolution were evaluated using a three-electrode configuration in 1 M KOH electrolyte, with the Hg/HgO as the reference electrode and a Pt plate as the counter electrode. The area of catalysts was 1 cm^2. The OER and

HER reactions were characterized by linear sweep voltammetry at a scan rate of 1 mV s^{-1} from negative to positive potential on the RHE scale, all polarization curves were corrected for IR losses. The C_{dl} values were determined by acquiring cyclic voltammograms at various scan rates (10, 20, 30, 40, 50, mV s^{-1}) in the non-faradaic region. The calculation of ECSA according to the method in the literature.[1] The stability of the electrodes was characterized by chronopotentiometry at 10、50、100 and 200 mA cm^{-2} current densities for 5 h.

The AEM cell measurements were performed on a DongHua DH7001 Electrochemical workstation. For overall two-electrode water splitting, $NiFeP_x$/Ni foam and NiFe LDH/Ni foam electrodes were used for hydrogen and oxygen evolution respectively, and the reaction was characterized by linear sweep voltammetry at a scan rate of 1 mV s^{-1} from 2 V to 1.3 V. 6 M KOH solution was used as the electrolyte and the flow was driven by a peristaltic pump. The Fumasep FAAM-15 anion exchange membrane was bought from SciMaterialsHub. The stability was characterized by chronopotentiometry at a current density of 300 mA cm^{-2} for approximately 100 h.

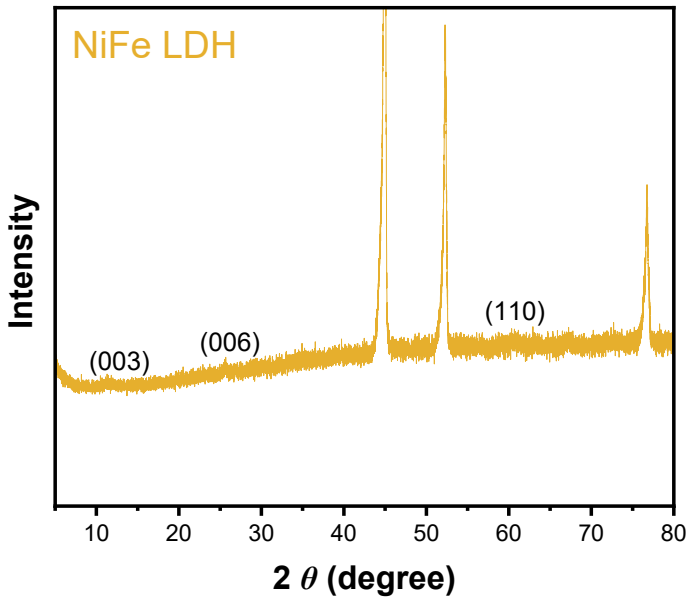

Figure S1. XRD pattern obtained for NiFe LDH on Ni foam.

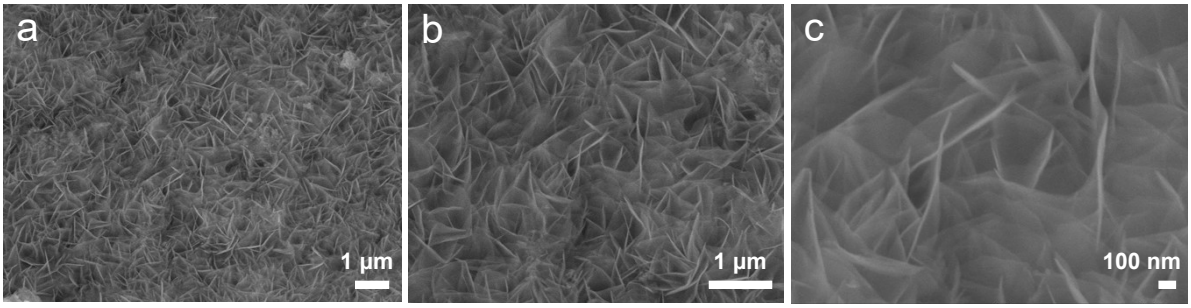

Figure S2. (a, b) Low-magnification and **(c)** high-magnification SEM images obtained for NiFe LDH on Ni foam.

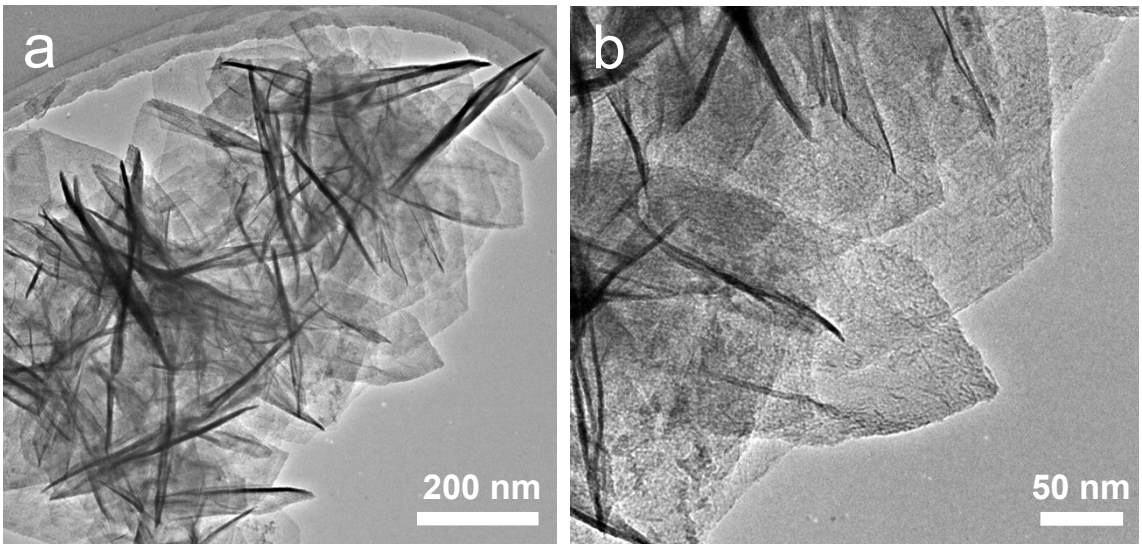

Figure S3. **(a, b)** Low-magnification TEM images obtained for NiFe LDH on Ni foam.

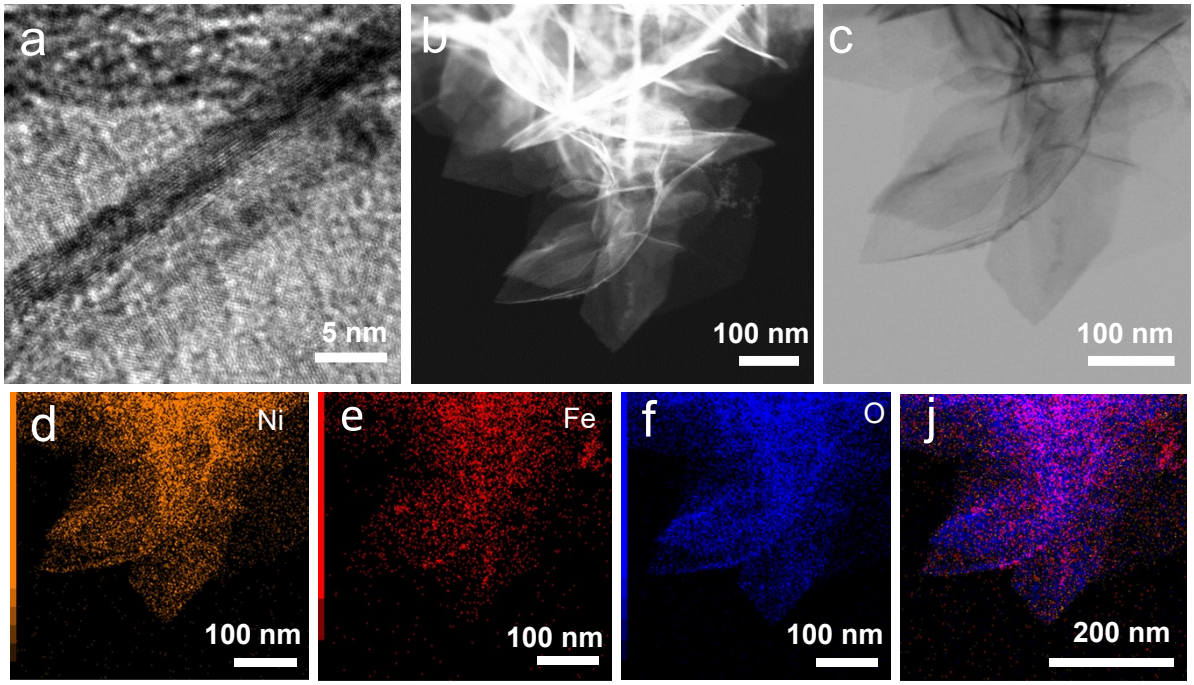

Figure S4. **(a)** HR-TEM **(b)** STEM images obtained for NiFe LDH and **(c-j)** Elemental mapping of NiFe LDH.

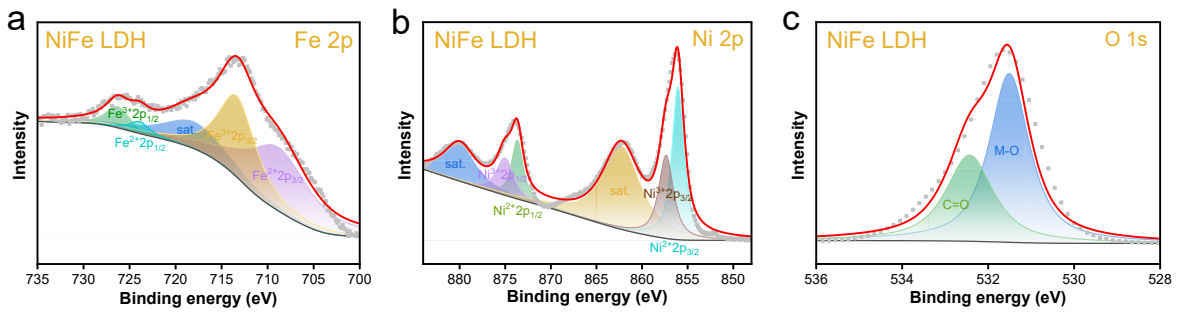

Figure S5. The high-resolution XPS spectra obtained for NiFe LDH **(a)** Fe 2*p*, **(b)** Ni 2*p*, and **(c)** O 1*s*.

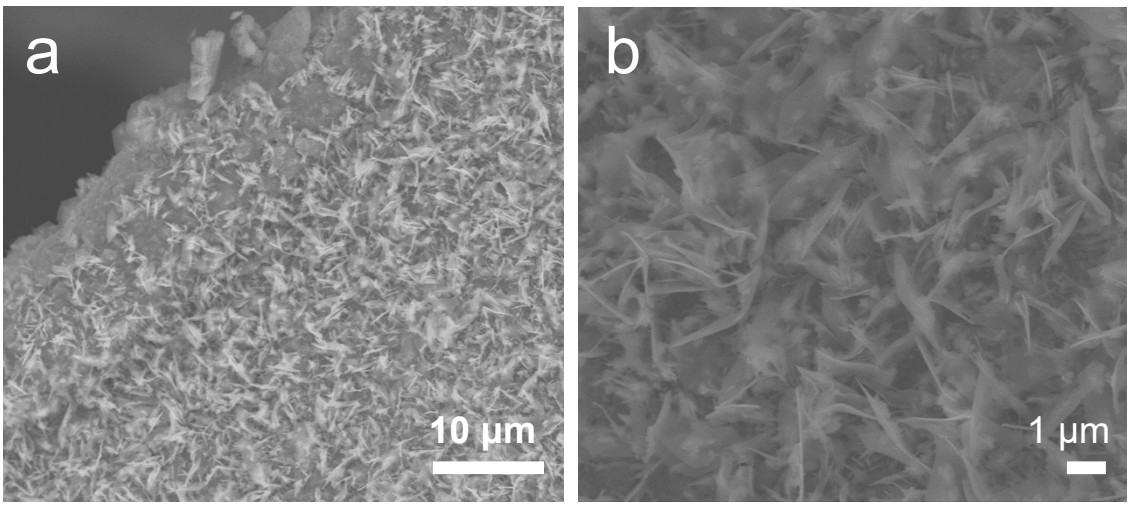

Figure S6. **(a)** Low- **(b)** High-magnification SEM images obtained for $NiFeP_x$ on Ni foam.

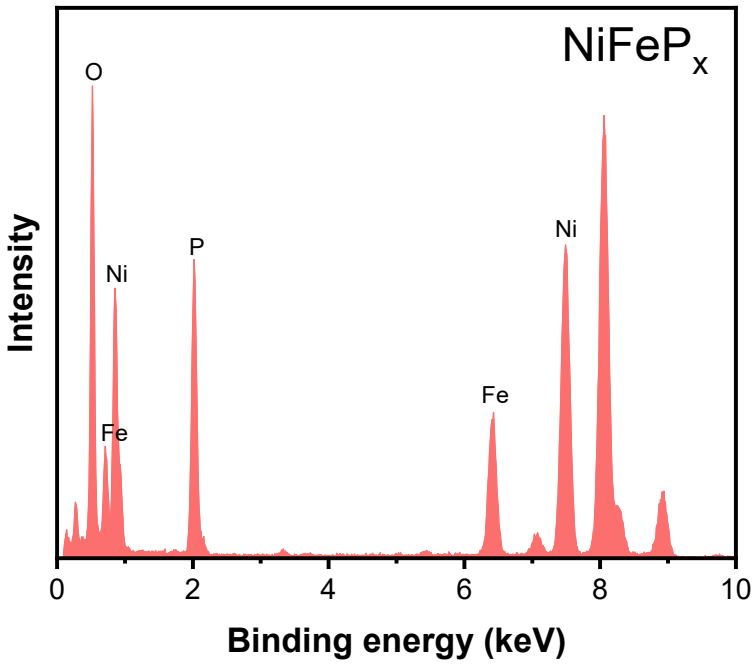

Figure S7. EDX spectrum obtained for $NiFeP_x$ on Ni foam.

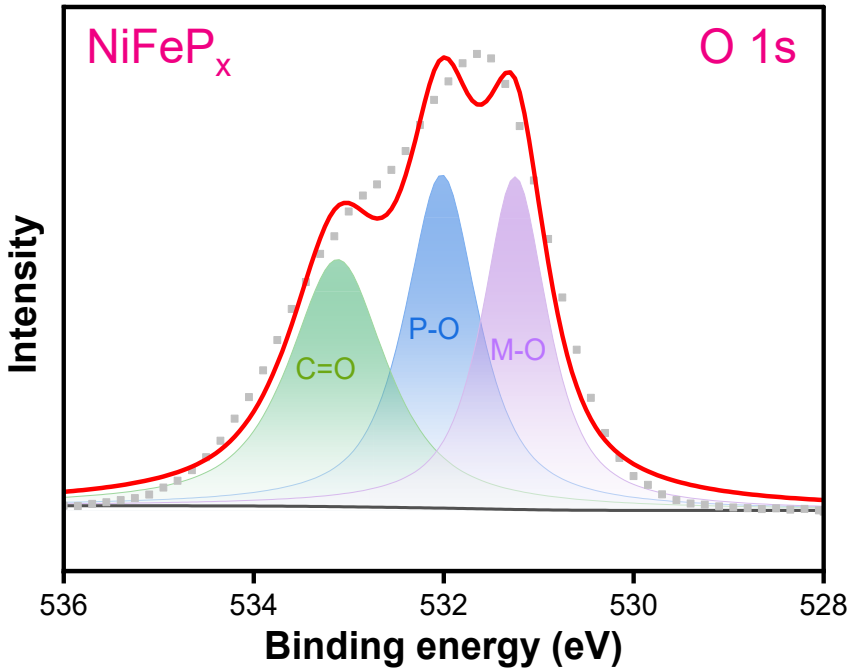

Figure S8. The high-resolution XPS spectrum obtained for O 2*p* for NiFeP$_x$.

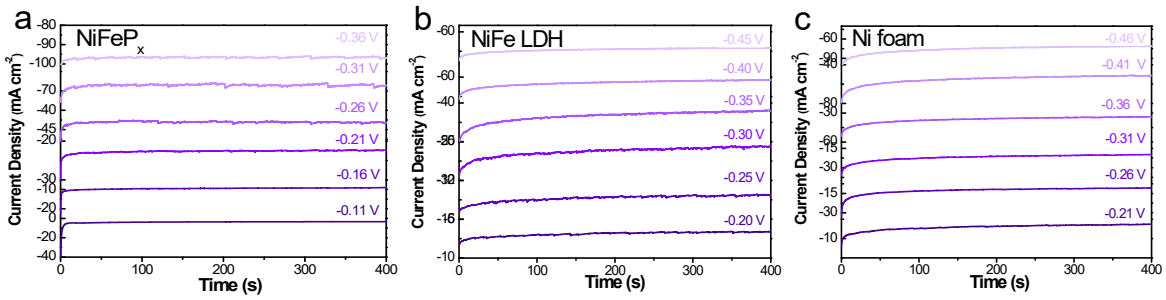

Figure S9. *I-t* curves were measured at different potentials for **(a)** $NiFeP_x$ **(b)** NiFe LDH and **(c)** Ni foam during the HER process.

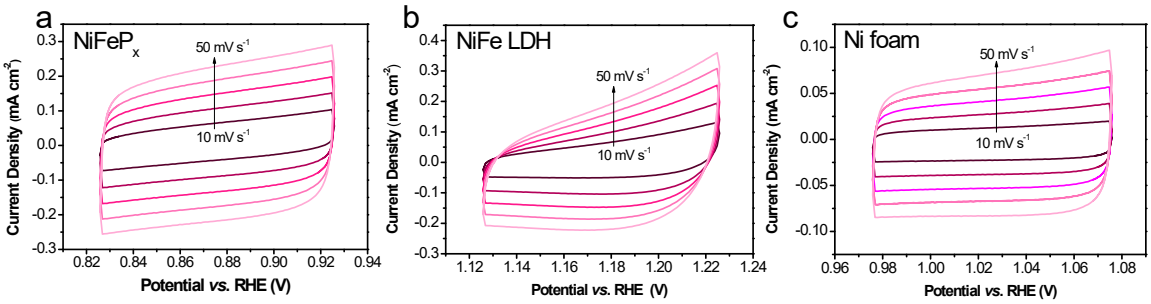

Figure S10. CV curves were measured for **(a)** $NiFeP_x$ **(b)** NiFe LDH **(c)** Ni foam at different scan rates.

Table S1. The ICP-OES data of NiFe LDH and $NiFeP_x$

	Fe	Ni	Ni/Fe
NiFe LDH	1.05%	96.99%	92.37%
$NiFeP_x$	1.00%	95.90%	95.90%

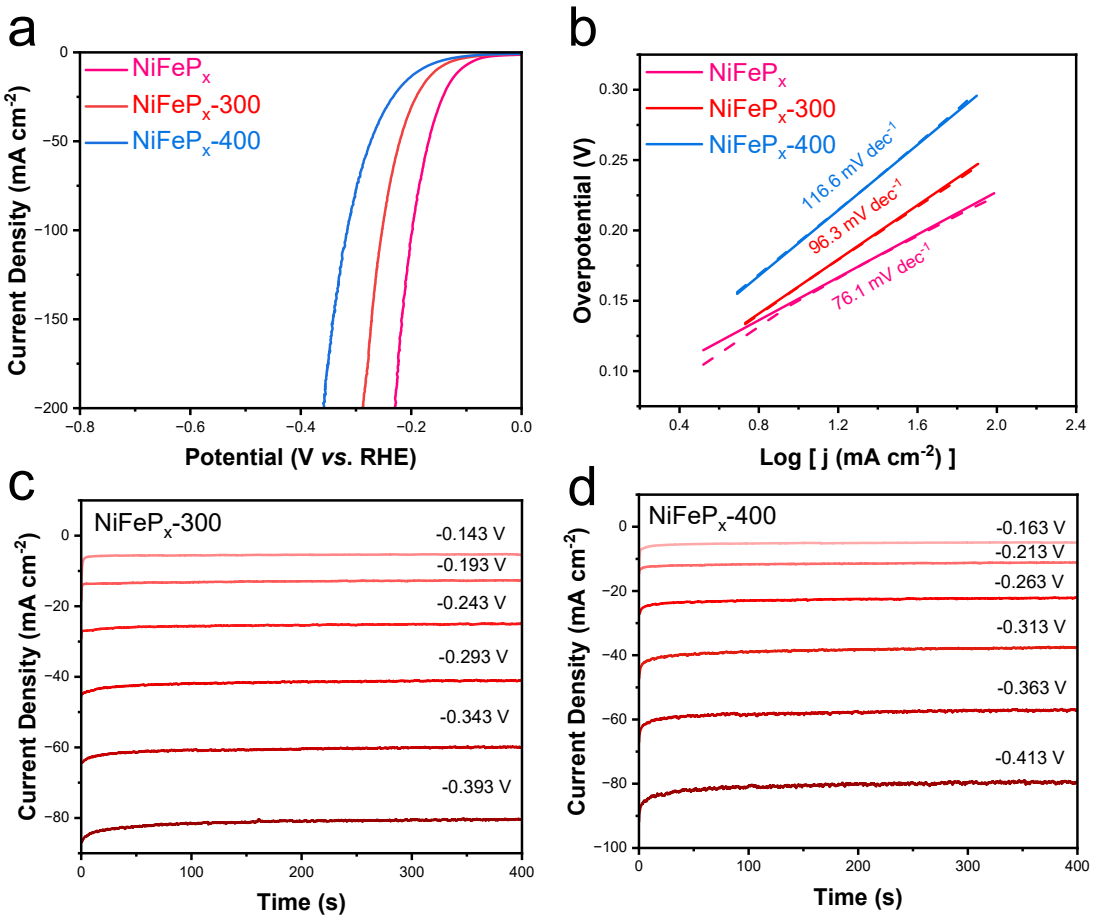

Figure S11. **(a)** Linear sweep voltammetry curves, **(b)** Tafel slopes of NiFeP$_x$, NiFeP$_x$-300, and NiFeP$_x$-400 (scan rate of 1 mV s^{-1}). *I-t* curves were measured at different potentials for **(c)** NiFeP$_x$-300, **(d)** NiFeP$_x$-400.

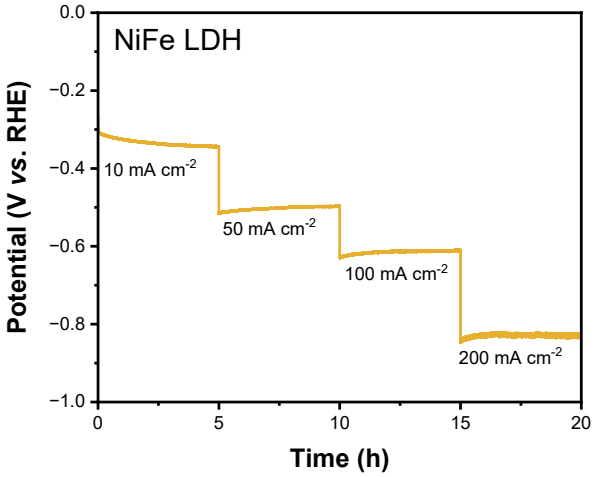

Figure 12. The *i-t* curve of NiFe LDH for HER.

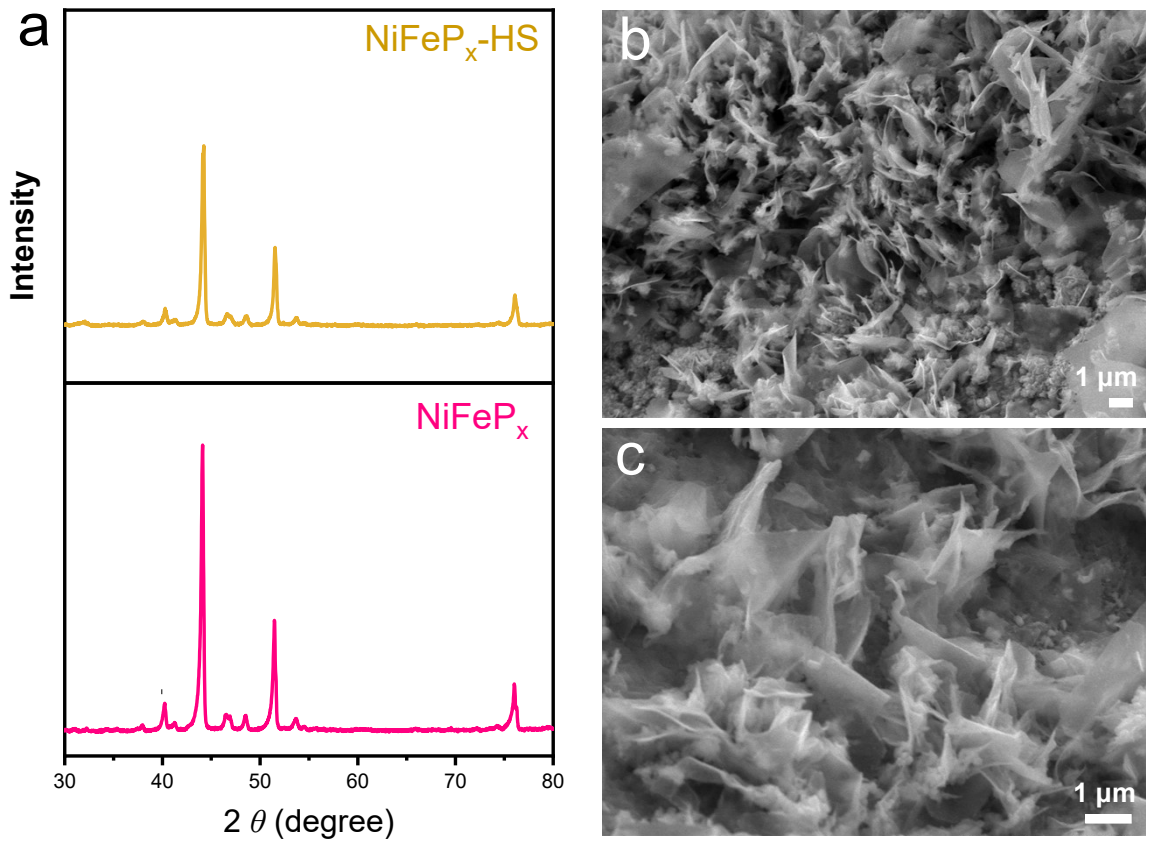

Figure S13. **(a)** XRD pattern measured for $NiFeP_x$ on Ni foam before and after HER stability test, **(b, c)** The Low-magnification SEM images obtained for $NiFeP_x$-HS.

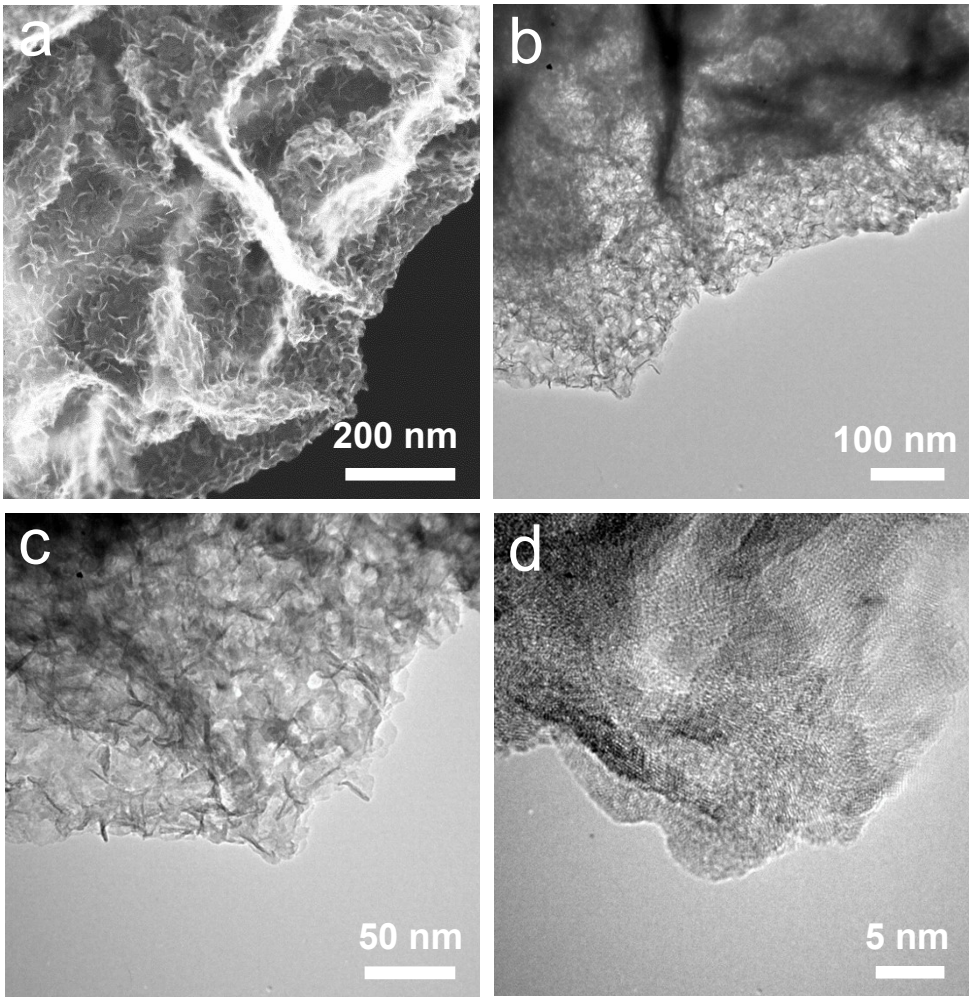

Figure S14. **(a, b, c)** Low-magnification and **(d)** high-magnification TEM images obtained for $NiFeP_x$-HS.

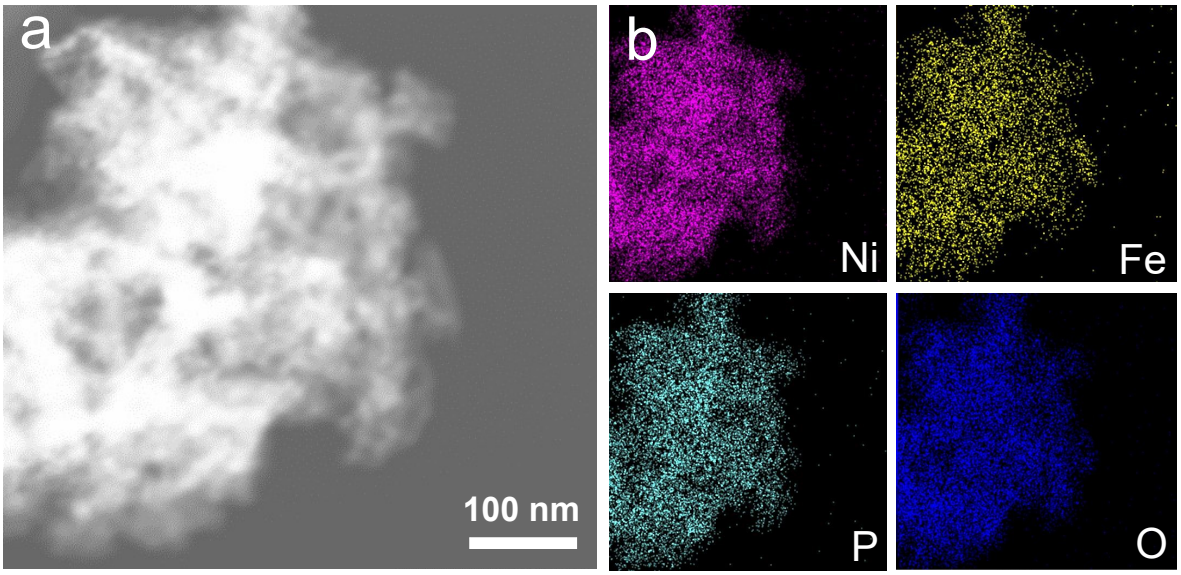

Figure S15. **(a)** STEM image obtained for $NiFeP_x$-HS and **(b)** the corresponding elemental mapping of the same area showing the distribution of Ni, Fe, P and O.

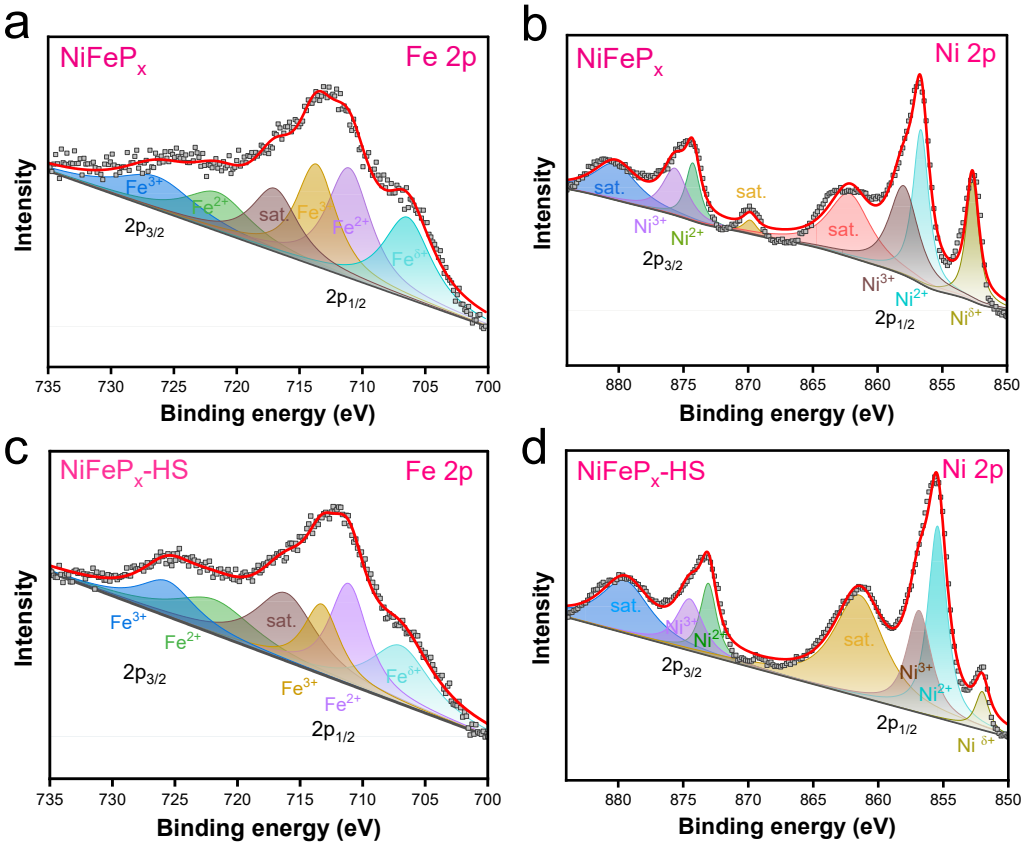

Figure S16. Comparison of high-resolution XPS **(a)** Fe 2*p* **(b)** Ni 2*p* spectra of $NiFeP_x$ and **(c)** Fe 2*p* **(d)** Ni 2*p* spectra of $NiFeP_x$-HS.

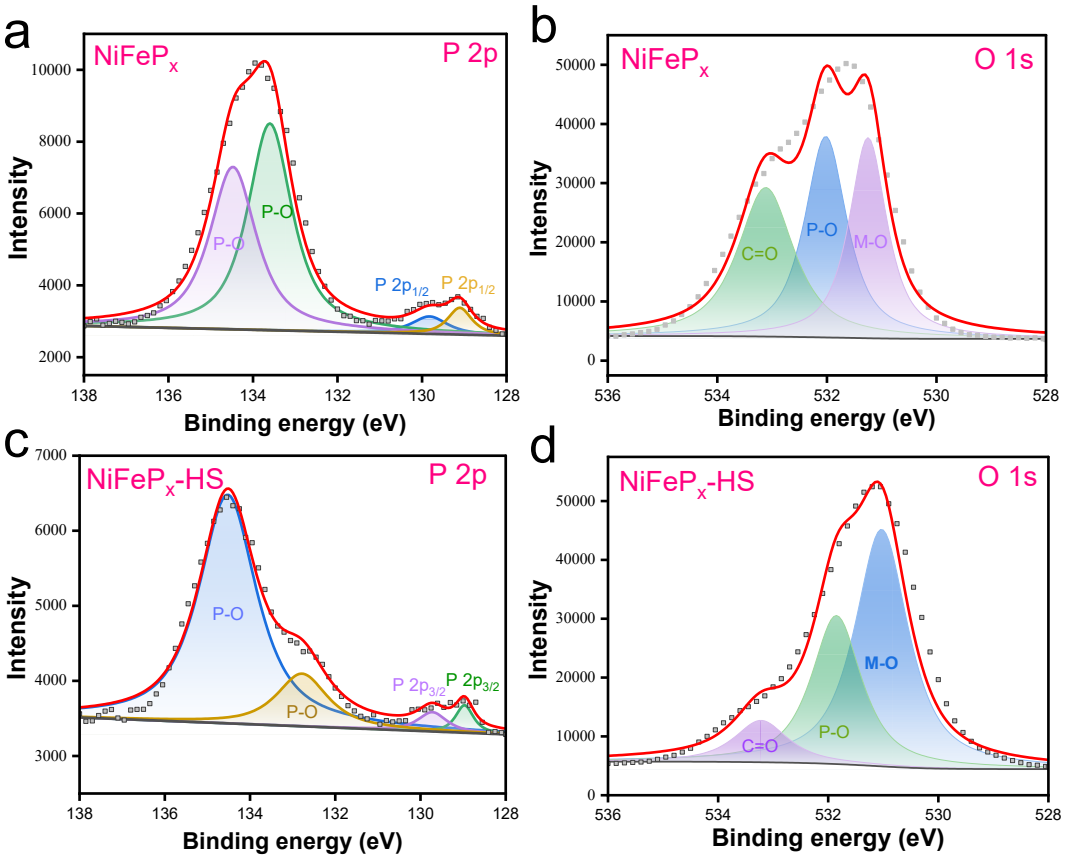

Figure S17. Comparison of high-resolution XPS **(a)** P 2*p* **(b)** O 1*s* spectra of $NiFeP_x$ and **(c)** P 2*p* **(d)** O 1*s* spectra of $NiFeP_x$-HS.

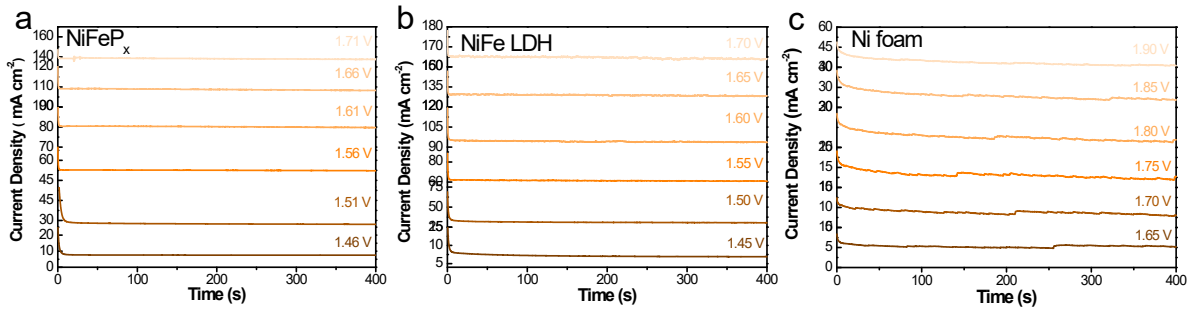

Figure S18. *I-t* curves were measured at different potentials for **(a)** $NiFeP_x$ **(b)** NiFe LDH **(c)** Ni foam during the OER process.

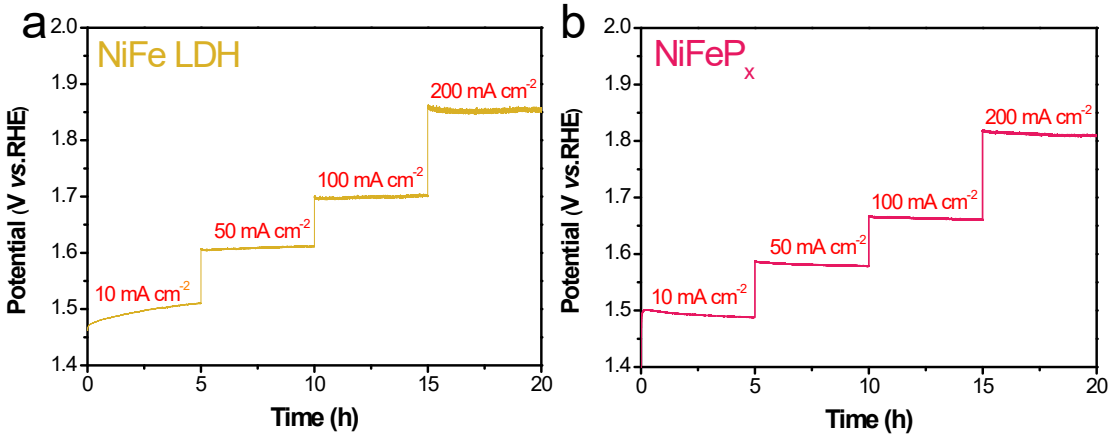

Figure S19. **(a)** *I-t* curves were measured for NiFe LDH on Ni foam and **(b)** $NiFeP_x$ on Ni foam during the OER process.

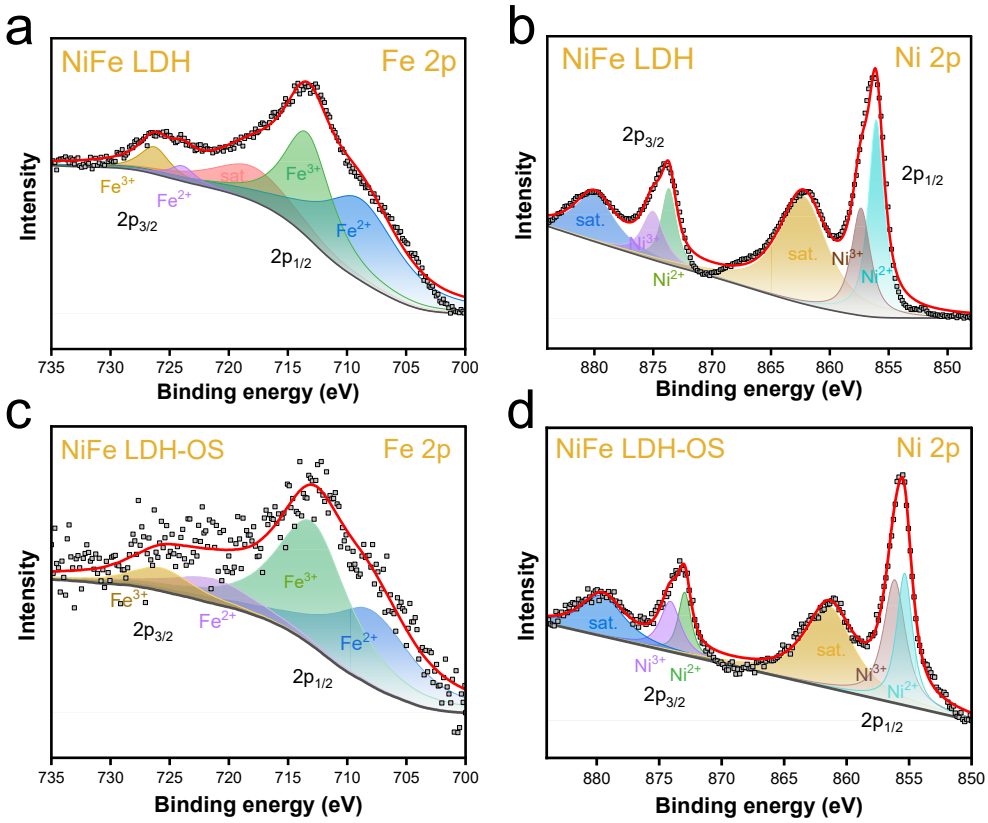

Figure S20. Comparison of high-resolution XPS **(a)** Fe 2*p* **(b)** Ni 2*p* spectra of NiFeP NiFe LDH and **(c)** Fe 2*p* **(d)** Ni 2*p* spectra of $NiFeP_x$-OS.

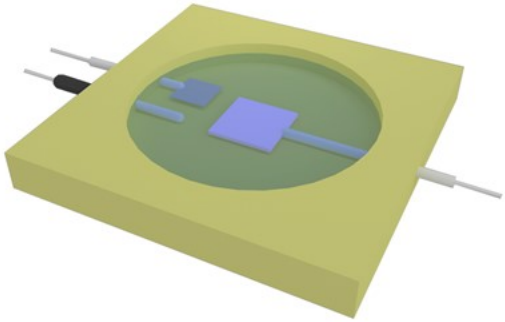

Figure S21. A schematic representation of the *in-situ* Raman device used to perform SERS measurements.

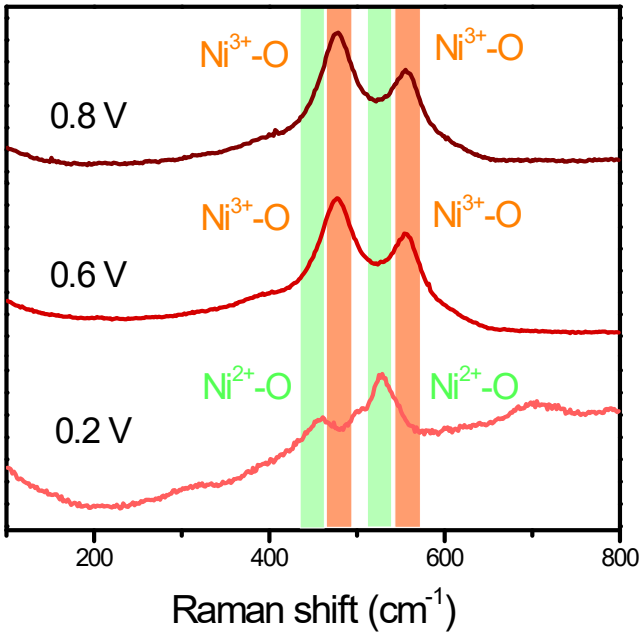

Figure S22. *In-situ* Raman of NiFe LDH during the OER process.

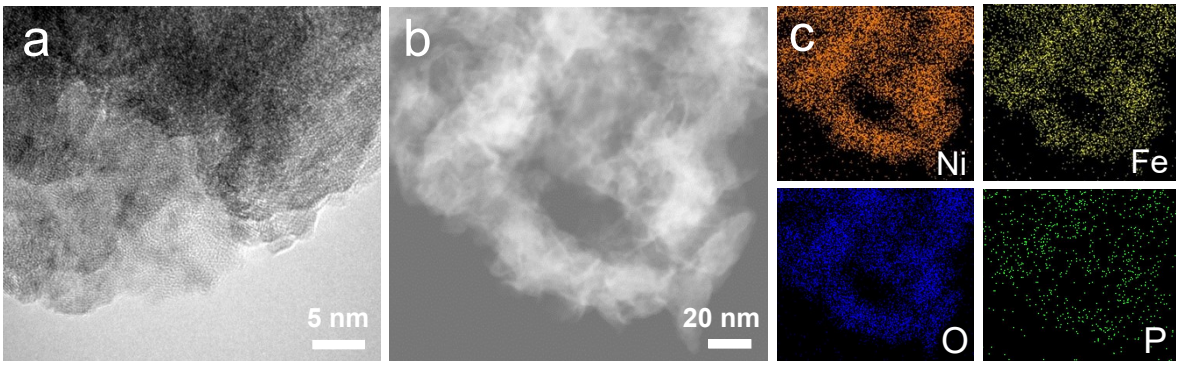

Figure S23. (a) HR-TEM **(b)** STEM image obtained for NiFe LDH and **(c)** Elemental mapping obtained for $NiFeP_x$-OS.

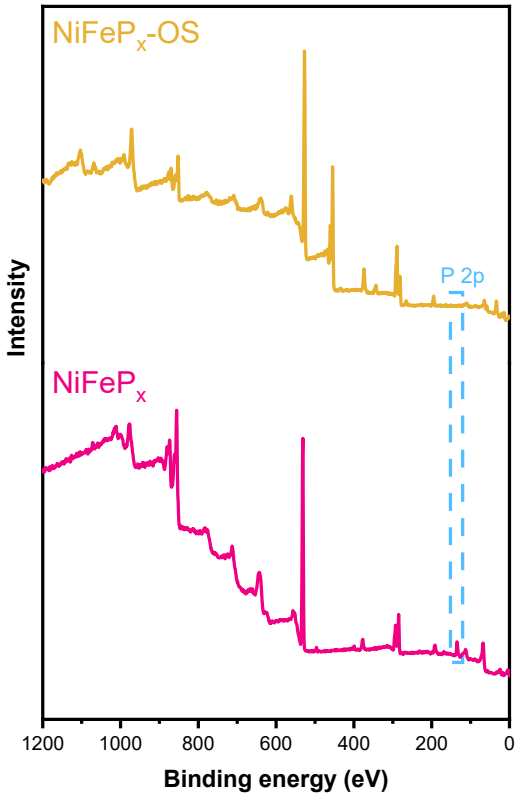

Figure S24. Survey XPS spectra measured for NiFeP$_x$-OS.

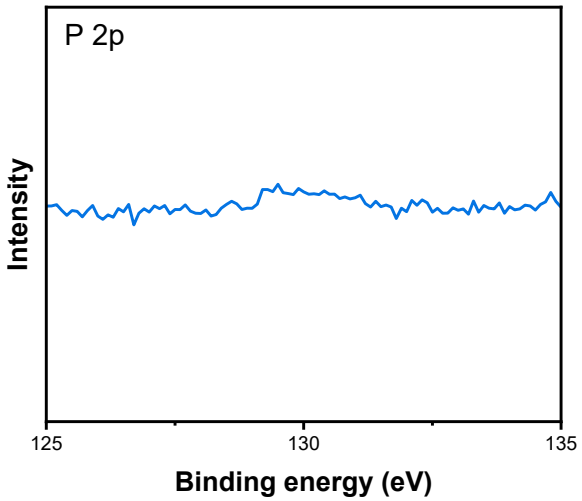

Figure 25. The high-resolution P 2*p* XPS spectra obtained for $NiFeP_x$-OS.

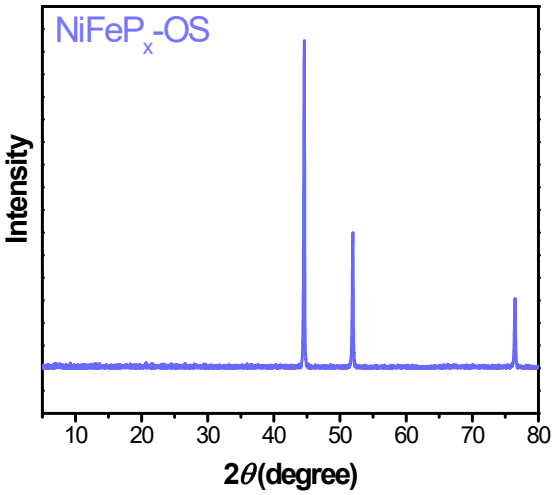

Figure S26. XRD pattern measured for $NiFeP_x$ measured after OER stability test.

Table S2. Comparison of the electrocatalytic HER performance of the electrode materials reported in this work with recently reported electrocatalysts in the literature.

No	Electrocatalysts	η_{10} (mV)	electrolyte	Ref.
	$NiFeP_x$	112	1 M KOH	This work
1	In-NiV LDH	114	1 M KOH	2
2	Co_2P/N-P	125	1 M KOH	3
3	N-FeS_2	126	1 M KOH	4
4	CNN-500	127	1 M KOH	5
5	$Ni_{1.5}Co_{1.5}P$/MFs	141	1 M KOH	6
6	Fe@Co-MOF-3	150	1 M KOH	7
7	Fe-Co_2P BNR	156	1 M KOH	8
8	sr-NiO	164	1 M KOH	9
9	Co SAs-Co NPs/NCFs	205	1 M KOH	10
10	$Fe_{50}Ni_{50}$ films	390	1 M KOH	11

References

1. Liang, H.; Gandi, A. N.; Anjum, D. H.; Wang, X.; Schwingenschlogl, U.; Alshareef, H. N. Plasma assisted synthesis of NiCoP for efficient overall water splitting. *Nano Lett*., 2016, **16**, 7718-7725.
2. He, D.; Cao, L.; Huang, J.; Kajiyoshi, K.; Wu, J.; Wang, C.; Liu, Q.; Yang, D.; Feng, L. In-situ optimizing the valence configuration of vanadium sites in NiV-LDH nanosheet arrays for enhanced hydrogen evolution reaction. *J. Energy Chem*., 2020, **47**, 263-271.
3. Jia, S.; Cheng, Y.; Huang, Q.; Li, Q.; Zhang, Q.; Wang, Z.; Zhang, Y.; Zhang, N.; Mu, Y. One-step synthesis of Co_2P/N-P co-doped porous carbon composites derived from soybean derivatives as acidic and alkaline HER electrocatalysts. *Int. J. Hydrogen Energy*, 2022, **47**, 24796-24806.
4. Ye, J.; Zang, Y.; Wang, Q.; Zhang, Y.; Sun, D.; Zhang, L.; Wang, G.; Zheng, X.; Zhu, J. Nitrogen doped FeS_2 nanoparticles for efficient and stable hydrogen evolution reaction. *J. Energy Chem*., 2021, **56**, 283-289.
5. Yan, Y.; Ma, Q.; Cui, F.; Zhang, J.; Cui, T. Carbon onions coated Ni/NiO nanoparticles as catalysts for alkaline hydrogen evolution reaction. *Electrochim. Acta*, 2022, **430**, 141090-141097.
6. Chen, T.; Qian, M.; Tong, X.; Liao, W.; Fu, Y.; Dai, H.; Yang, Q. Nanosheet self-assembled NiCoP microflowers as efficient bifunctional catalysts (HER and OER) in alkaline medium. Int. *J. Hydrogen Energy*, 2021, **46**, 29889-29895.
7. Dai, S.; Liu, Y.; Mei, Y.; Hu, J.; Wang, K.; Li, Y.; Jin, N.; Wang, X.; Luo, H.; Li, W. Iron-doped novel Co-based metal-organic frameworks for preparation of bifunctional catalysts with an amorphous structure for OER/HER in alkaline solution. *Dalton T*., 2022, **51**,15446-15457.
8. Lin, Y.; Sun, K.; Chen, X.; Chen, C.; Pan, Y.; Li, X.; Zhang, J. High-precision regulation synthesis of Fe-doped Co_2P nanorod bundles as efficient electrocatalysts for hydrogen evolution in all-pH range and seawater. *J. Energy Chem*., 2021, **55**, 92-101.
9. Yi, X.; He, X.; Yin, F.; Li, G.; Li, Z. Surface strain engineered Ni-NiO for boosting hydrogen evolution reaction in alkaline media. *Electrochim. Acta*, 2021, **391**, 138985-138994.

10. Wang, M.; Li, M.; Zhao, Y.; Shi, N.; Zhang, H.; Zhao, Y.; Zhang, Y.; Zhang, H.; Wang, W.; Sun, K.; et al. Construction of N-doped carbon frames anchored with Co single atoms and Co nanoparticles as robust electrocatalyst for hydrogen evolution in the entire pH range. *J. Energy Chem*., 2022, **67**, 147-156.
11. Perez Bakovic, S. I.; Acharya, P.; Watkins, M.; Thornton, H.; Hou, S.; Greenlee, L. F. Electrochemically active surface area controls HER activity for Fe_xNi_{100-x} films in alkaline electrolyte. *J. Catal*., 2021, **394**, 104-112.